Quantifying Southern Oscillation–Precipitation Relationships from an Atmospheric GCM

THOMAS M. SMITH AND CHESTER F. ROPELEWSKI

National Centers for Environmental Prediction, Climate Prediction Center, NWS/NOAA, Camp Springs, Maryland

(Manuscript received 27 September 1996, in final form 24 January 1997)

ABSTRACT

This paper is an extension of a study by C. Ropelewski and M. Halpert, which examines observed precipitation relationships with the Southern Oscillation. Here, the authors repeat their analysis using atmospheric general circulation model precipitation from the average of a 13-run ensemble. The GCM is the atmospheric component of the coupled model used for seasonal prediction at the National Centers for Environmental Prediction, except that in this study, the observed sea surface temperatures were specified for the ensemble runs. Results are compared and contrasted with the observed Southern Oscillation–related precipitation behavior. These comparisons show that the multiple ensemble simulations compare favorably to the observations for most areas in the Tropics and subtropics. However, outside of the deep Tropics, the model simulations show large shifts or biases in the location of the Southern Oscillation–related anomalies. In particular, anomalies shown by the observations to occur in the southeastern United States are shifted westward in the simulation.

1. Introduction

In an earlier study, Ropelewski and Halpert (1996, hereafter RH) examined the relationships between the distributions of observed precipitation amounts and the Southern Oscillation (SO). They discussed SO–precipitation relationships for a number of previously identified regions for which there were sufficient data. Here, we repeat their analysis using precipitation derived from an atmospheric general circulation model. As in RH, we fit the precipitation to a gamma distribution and compare percentiles for high and low SO index periods. The GCM is the atmospheric component of the coupled atmosphere–ocean model used at the National Centers for Environmental Prediction (NCEP) for seasonal predictions. Therefore, comparisons of these results to RH gives an indication of the coupled model's potential for generating useful seasonal predictions without resorting to bias corrections and/or statistical adjustments.

The precipitation used for this study is from a 13-ensemble average of atmospheric GCM simulations made at NCEP. Each ensemble is an extended GCM simulation with identical boundary forcing but slightly different initial conditions, covering the period 1951–94. The model is forced by the specified sea surface temperature of Smith et al. (1996) through 1981 and the SST described by Reynolds and Smith (1994) afterward. Seasonal means derived from monthly average precipitation for the ensemble are examined here. The atmospheric GCM is a T40 (approximately 2.8° lat × 2.8° long) version of the NCEP medium-range forecast model, which has been tuned to more accurately simulate tropical convection (Ji et al. 1994; Kumar et al. 1996).

Analysis of the GCM precipitation from individual ensembles over the contiguous United States (Livezey et al. 1997) has shown that the model's internal variability of precipitation is reasonable. Using an ensemble will tend to lower the overall variance compared to analyzing an individual run by averaging out internal variability, but climatic anomalies associated with the SST forcing should be retained. The ensemble size is large enough to clearly show the GCM climate signal forced by the SST boundary condition. Since our goal is to investigate the GCM precipitation variations associated with SST forcing, we do our analysis on the ensemble mean rather than on individual runs. The analysis of the ensemble mean is also consistent with operational seasonal prediction procedures.

2. Results

As with the observations in RH, the model precipitation is first averaged into seasons of 3 or more months and then fit to a gamma distribution. We define year 0 to be the year of the beginning of the SO extreme and year + to be the following year. The SO high- and low-index years are the same as in RH, except that our period begins in 1951 and the low-index year 1992 was added.

Corresponding author address: Dr. Thomas M. Smith, Analysis Branch, Climate Prediction Center, National Centers for Environmental Prediction, World Weather Building, 5200 Auth Road, Room 605, W/NP52, Camp Springs, MD 20746.
E-mail: wd52ts@sgi25.wwb.noaa.gov

TABLE 1. List of 11 warm and 8 cold Southern Oscillation episodes used in this study (1951–1994). The four digits of the SO episode year 0 are listed.

Warm (low SO index) years	1951, 1953, 1957, 1965, 1969, 1972, 1976, 1982, 1986, 1991, 1992
Cold (high SO index) years	1955, 1956, 1964, 1970, 1971, 1973, 1975, 1988

Table 1 lists the high- and low-index years, where the year listed is the year of an episode or the first year of a multiyear episode.

Seasonal area average precipitation for high-index and low-index years, and for the 1961–90 base period, are separately fit to gamma distributions. From those fits, we determine the values of the 10th, 30th, 50th, 70th, and 90th percentiles as a function of SO extreme for display in box and whisker plots and tables. Box and whisker plots show the median by the horizontal line across the box. The 30th and 70th percentiles are shown by the lower and upper edges of the box respectively, and the 10th and 90th percentile by the lower and upper ends of the vertical whisker lines that pass through the box. Confidence levels are assessed by counting the number of high- (or low) index years that have less than the climatological level of precipitation and comparing that number to the probability of it occurring with a random distribution. The probability that k randomly selected years, out of a set of n years, is less than the climatological value can be expressed by

$$P(k)_{\text{Ran}} = \frac{\binom{n}{k}}{\sum_{j=0}^{n} \binom{n}{j}}.$$

Note that this only gives the probability that the model is consistently placing a precipitation anomaly of the same sign in a location for a given SO index sign. It says nothing about the accuracy of the model precipitation.

In a companion analysis, percentiles are computed at each location on the map using all seasonal data, and then composite maps are formed by averaging over the high- and low-index years to show the spatial structure of the relationships.

a. Spatial structure of SO model–precipitation relationships

Since model output is not as spatially limited as observed data, we are able to show global SO-related precipitation percentiles, instead of only those over land surfaces as discussed by RH. We show the percentiles globally for two seasons, Apr(0)–Sep(0) and Oct(0)–Mar(+), averaged for both low- and high-index periods (Fig. 1). For most regions defined by RH, this choice of seasons simplifies the analysis and minimizes the splitting of the season of SO-related precipitation. Comparisons of these model-based percentiles for these two seasons, with percentiles formed using the more precise definition of the season used by RH, show only slight differences.

During low-index periods, the model ensemble average composites for both seasons show enhanced precipitation in the equatorial and tropical South Pacific. For the Apr(0)–Sep(0) season, the low-index model composite precipitation is also enhanced across the North Pacific near 40°N and in the eastern Mediterranean region. Drier regions associated with a low index in both seasons include the Australia–Indonesia region. Model composites for Oct(0)–Mar(+) show that southern Africa and northern South America also tend to be drier during low-index years. While the compromise averaging seasons chosen may not be optimal for those two regions, the results are qualitatively the same as when the carefully chosen averaging seasons in RH are used.

For the high-index composites, precipitation percentiles roughly mirror those for low-index composites in many regions. Part of the symmetry could be artificial because of the ways we formed the composites. This symmetry is most apparent in the tropical Pacific, but it also occurs over northern South America and southern Africa in Oct(0)–Mar(+) and over the eastern Mediterranean region in Apr(0)–Sep(0). Over the western Mediterranean, dry conditions appear in both the Apr(0)–Sep(0) and the Oct(0)–Mar(+) high-index composites.

While precipitation percentile patterns in Fig. 1 are largely symmetric with SO phase, there are regions where the SO relationships are not colinear (i.e., they are larger for one sign of the SO index than for the other). For example, the Apr(0)–Sep(0) percentiles over northern Australia have high-index percentiles that are more extreme than their low-index percentiles. This may be a reflection of the fact that April to September is usually a very dry season and any precipitation is likely to be reflected in large percentile values. However, the model consistently shows larger areas of extremes associated with high-index years compared to low-index years. Since this asymmetry is not apparent in the observations of RH over the limited regions where observations are available, it most likely reflects a model bias. For the regions of extreme model percentiles discussed above, the high–low percentiles are significant at the 90% level. The precipitation extremes over regions for which RH were able to compute percentiles from observations are discussed below. Over some regions, such as over the oceans, there are insufficient observed data to adequately compare the model with precipitation–SO relationships.

Comparison of satellite-based precipitation estimates [i.e., estimates based on observations of outgoing longwave radiation (OLR)] for their shorter record length (1973–92) helps to confirm model SO–precipitation re-

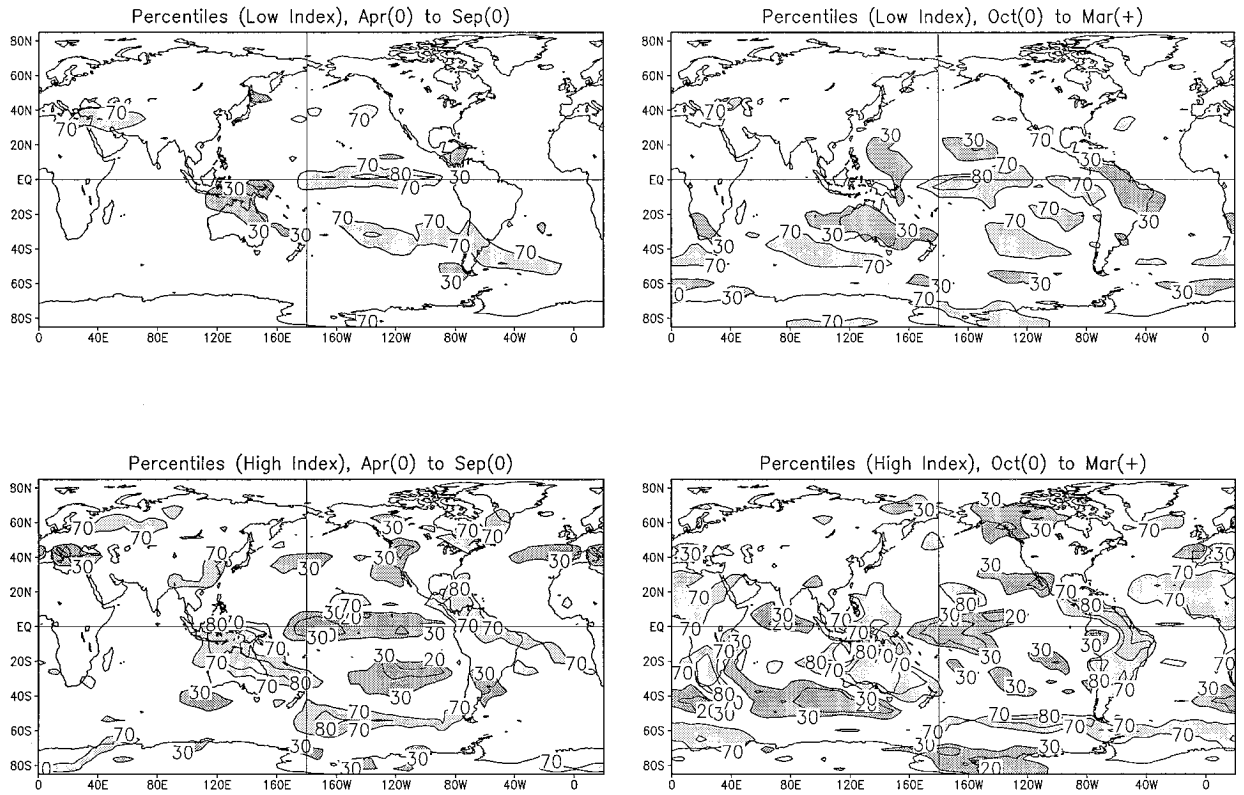

FIG. 1. Global model precipitation percentiles based on the 1951–94 period, averaged for low-index years (top) and high-index years (bottom). Averaging seasons are Apr(0)–Sep(0) (left) and Oct(0)–Mar(+) (right). Percentiles <30 are shaded dark, percentiles >70 are shaded light, and percentiles of 20, 30, 70, and 80 are contoured.

lationships over the oceans. The model analysis over the central to west Pacific and northeastern South America is consistent with differences between satellite-derived tropical rainfall for one set of low- and high-index periods, 1987 minus 1988 for summer and winter (Janowiak and Arkin 1991). Monthly averaged OLR since 1974 (not shown) is consistent with model-estimated precipitation (Fig. 1) for the tropical Pacific and northeastern South America. However, in general, the model tends to concentrate SO-related variations too far east compared to the OLR in the region from Indonesia to India. The model ensemble composites also show larger regions with large precipitation anomalies during the high-index phase than during the low-index phase, while the observations do not show that asymmetry. This may be due to the relatively low number of warm and cool events available for this study, as well as model bias.

To supplement the global analysis, we also examine precipitation percentile composite maps for two regions, southern Asia–Australia (Fig. 2) and the Americas (Fig. 3). For these regions, we contour and shade the 40th and 60th percentiles to enhance detailed differences of composite model behavior. This more detailed analysis clearly shows the model composite percentile differences associated with the SO over India (Fig. 2), where the signal is consistent and significant but relatively small (Rasmusson and Carpenter 1983; Shukla and Paolino 1983). The variations in Apr(0)–Sep(0) model composite Indian monsoon precipitation are shifted slightly north from where the observations place them. Over southern India and Sri Lanka, the Oct(0)–Mar(+) signal is also generally consistent with Rasmusson and Carpenter (1983) and Shukla and Paolino (1983) in showing dry conditions, but it misses the low-index extreme wet conditions. The model's Indian subcontinent percentiles are only significant at the 90% level over northern India.

Model composites show a precipitation relationship over southern to eastern China for the Oct(0)–Mar(+) season, which is wetter than normal in low-index periods. In high-index periods, southern China is drier than normal for the Oct(0)–Mar(+) season, which is normally the dry season in east Asia. These SO relationships were suggested in the correlation studies of Kiladis and Diaz (1989), but they did not meet the more stringent requirements of RH. The region is generally not significant at the 90% level.

Over the Gulf of Mexico region, RH show enhanced precipitation in the low-index phase and drier conditions in the high-index phase for the Oct(0)–Mar(+) season. The model ensemble composites show westward and southward shifts in the percentile pattern (which are

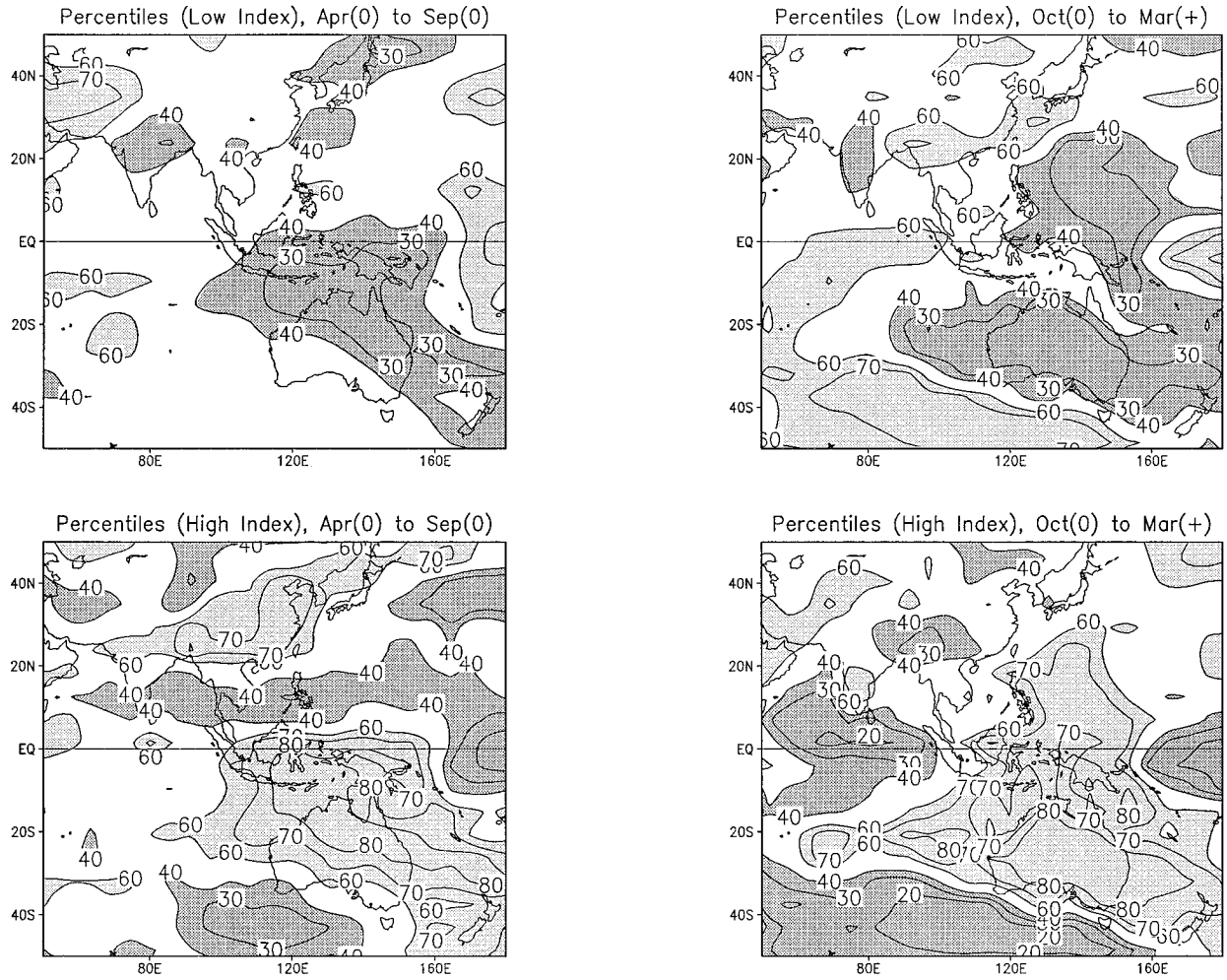

FIG. 2. As in Fig. 1 except between 50°E and 180°, 50°S and 50°N. Percentiles <40 are shaded dark, percentiles >60 are shaded light, and percentiles of 20, 30, 40, 60, 70, and 80 are contoured.

significant at the 90% level) compared to observations (Fig. 3). In the model composites, northwest North America has a strong dry signal associated with high-index periods in both seasons, which was not consistently evident in the observations.

For southern South America (Fig. 3), there is symmetry about the SO of the percentiles in both Apr(0)–Sep(0) and Oct(0)–Mar(+). For the Apr(0)–Sep(0) season, these model relationships are similar to those in RH for the Jun(0)–Oct(0) season. In RH, the low-index anomalies for the Nov(0)–Feb(+) season are less consistent with the model Oct(0)–Mar(+) anomalies because of a southward shift of the model anomalies relative to the observations. However, the overall consistency between the observations and the model in southern South America is encouraging, but the season differences and slight regional shifts are important. Over Central America, the GCM is also consistent with the observations, but the relationship there is stronger and more symmetric than shown by RH using observations. The GCM's southern South America signal is only weakly consistent from event to event, while the Central American signal shows much more consistency in the sign of the precipitation anomaly as a function of the SO phase.

b. Regional average SO model–precipitation relationships

In this section, we form model composite precipitation distributions for the seasons and regions identified by RH and compare them to the observations. The regions are shown in RH (their Fig. 1). Their seasons for averaging are repeated here, shown for some regions in Table 2. Here, for each season and region, the model composite percentiles are computed for the high-index years, the low-index years, and the base period years 1961–90.

For each of the regions in the Americas, discussed below, RH show large shifts in the observed precipi-

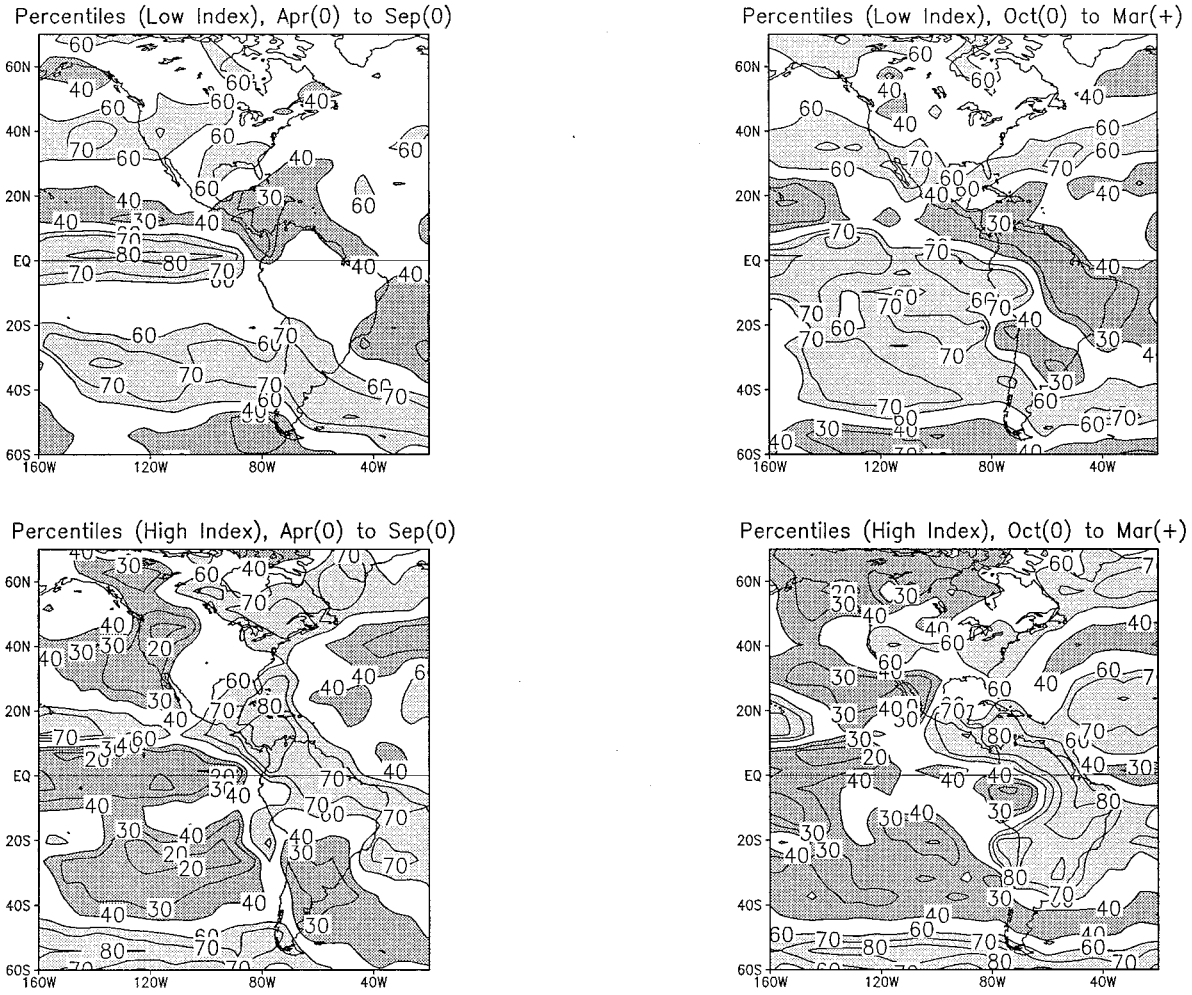

FIG. 3. As in Fig. 1 except between 160° and 20°W, and 60°S to 70°N. Percentiles <40 are shaded dark, percentiles >60 are shaded light, and percentiles of 20, 30, 40, 60, 70, and 80 are contoured.

tation as a function of SO phase. For Jul(0)–Mar(+) in northeastern South America, Fig. 4 clearly shows model SO relationships similar to the observed relationships in RH, which are consistent with Chu (1991). For data averaged over southeastern South America (Table 2), the model shows no net response to warm and cool episodes. For Oct(0)–Mar(+) in the Gulf of Mexico, the observations in RH show a clear SO modulation for both phases, where high-index extremes are not apparent in the model (Fig. 5). The spatial patterns for the Oct(0)–Mar(+) season (Fig. 3) show the symmetry of the SO relationship across South and Central America. However, as noted above, the model SO-related percentiles pattern is shifted south and west into northwestern Mexico.

The model's precipitation percentiles for the Indian subcontinent (Fig. 6) do not show the observed symmetry associated with the SO, in part because the model shows a strong north–south gradient in the high-index percentiles. The model percentiles for the area average precipitation for the low-index years are only slightly lower than those for the base years, and for high-index years they are about the same as those for the base years. Figure 2 shows that the strongest model signal is in the northern part of India. If we include only the northern part of India, a closer agreement to observations is obtained (not shown).

In the central Pacific, the strong observed relationship between the SO and precipitation is also reflected in the model precipitation (Fig. 7). The relationship using data averaged over Hawaii (Table 2) is also consistent with RH. Both the Oct(0)–Mar(+) and the Apr(0)–Sep(0) seasons (Fig. 1) show the symmetric SO relationship across the tropical Pacific. In contrast, the model distributions for the Fiji–New Caledonia region (Fig. 8) show a much weaker relationship than the observations in RH. In the model, the Fiji–New Caledonia region of the southwestern Pacific is between the areas of low and high precipitation associated with different phases of the SO (Fig. 1). Thus, subtle errors in the location of

TABLE 2. Anomalous precipitation rates from observations of RH (Obs) compared to the GCM, expressed as a percentage change from median during the base period. For the GCM, the consistency significance level is also given in parentheses, with values >0.99 denoted as 0.99.

Region	Season	Low SO index		High SO index		
Central Pacific	Mar(0)–Mar(+)	+83%		−45%		Obs
		+34%	(0.99)	−34%	(0.99)	GCM
South-central Pacific	Aug(0)–Jun(+)	+17%		−19%		Obs
		+27%	(0.99)	−24%	(0.99)	GCM
Fiji–New Caledonia	Oct(0)–Mar(+)	−20%		+32%		Obs
		−3%	(0.77)	−3%	(0.89)	GCM
Hawaii	Nov(0)–Apr(+)	−26%		+20%		Obs
		−19%	(0.99)	+15%	(0.99)	GCM
Micronesia–western Pacific	Oct(0)–May(+)	−20%		+16%		Obs
		−9%	(0.92)	+3%	(0.78)	GCM
Indonesia–New Guinea	Jul(0)–Nov(0)	−18%		+20%		Obs
		−17%	(0.99)	+35%	(0.99)	GCM
Northern Australia	Sep(0)–Jan(+)	−21%		+28%		Obs
		−18%	(0.99)	+28%	(0.99)	GCM
Southeastern Africa	Nov(0)–Apr(+)	−9%		+9%		Obs
		−4%	(0.97)	+5%	(0.99)	GCM
Eastern equatorial Africa	Nov(0)–Mar(+)	+12%		−9%		Obs
		−6%	(0.84)	+6%	(0.97)	GCM
Gulf of Mexico coast	Oct(0)–Mar(+)	+18%		−14%		Obs
		+5%	(0.97)	+1%	(0.73)	GCM
Northeastern South America	Jul(0)–Mar(+)	−15%		8%		Obs
		−12%	(0.99)	+14%	(0.99)	GCM
Southeastern South America (low index)	Nov(0)–Feb(+)	+16%		−19%		Obs
(high index)	Jun(0)–Oct(0)	0%	(0.84)	−3%	(0.78)	GCM

the model's South Pacific convergence zone may account for the differences between the model and observations.

Farther west, over Australia and much of Indonesia, the model's SO–precipitation relationship is clear, as shown by Fig. 1 for Oct(0)–Mar(+), and is consistent with RH. Another region of persistent SO-related anomalies found by RH is southeastern Africa. Again, for Oct(0)–Mar(+), Fig. 1 shows that the model simulates this behavior. Using data averaged over southeastern Africa, the model's percentiles (Table 2) are consistent with the observations reported by RH where there is a well-known relationship with the SO. However, in eastern equatorial Africa, where RH show a relationship with the SO, the model has an opposite relationship (Table 2), perhaps because of the model's tendency to regionally shift rainfall.

With the exception of eastern equatorial Africa, the area-averaged precipitation anomalies are consistent at the 90% level where the signals are strong. Areas with weak or shifted percentile signals generally also have low significance levels. The inconsistency in the signal over eastern equatorial Africa suggests that the model needs to be improved before it is useful for that region.

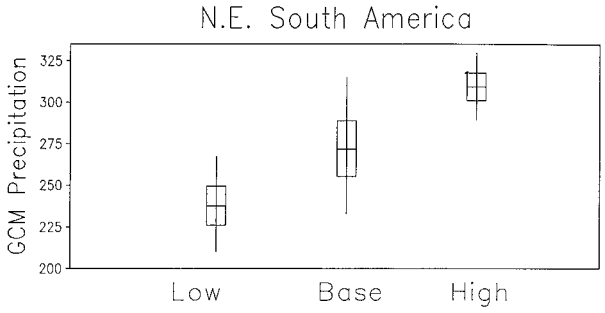

FIG. 4. Box and whisker plots for model precipitation averaged in northeastern South America for low-index years, base period years, and high-index years. Indicated for each are the 50th percentile (horizontal line through the box middle), the 30th and 70th percentiles (lower and upper edges of the box), and the 10th and 90th percentiles (lower and upper ends of the vertical whisker line). The averaging season is Jul(0)–Mar(+). Units are mm of precipitation month^{-1}.

3. Summary and conclusions

We have analyzed the predictability of an atmospheric GCM for global precipitation, compared to observations, to show what may be expected when this atmo-

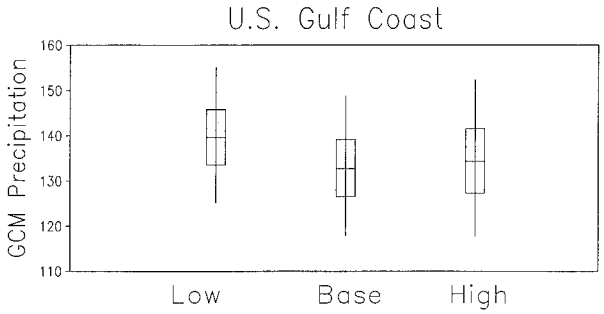

FIG. 5. As in Fig. 4 except for the U.S. Gulf Coast. The averaging season is Oct(0)–Mar(+).

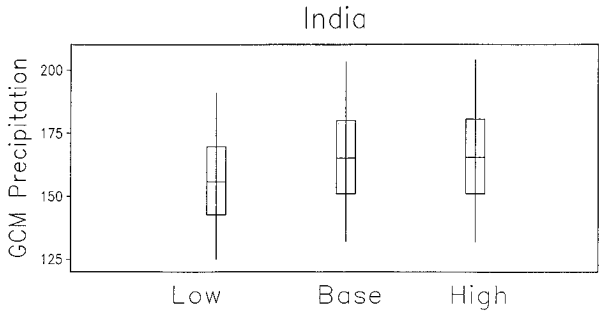

FIG. 6. As in Fig. 4 except for India. The averaging season is Jun(0)–Sep(0).

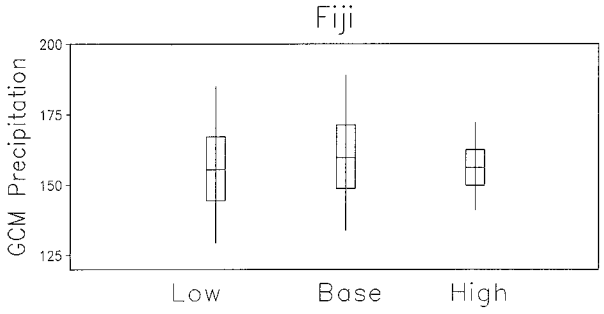

FIG. 8. As in Fig. 4 except for the Fiji–New Caledonia region. The averaging season is Oct(0)–Mar(+).

spheric GCM is coupled to an ocean GCM for seasonal forecasting. Since the GCM ensemble used here employs observed SST, this may be thought of as an upper bound on coupled model skill. Our goal is not just to evaluate this particular model, but also to encourage interest in further studies of the general problem of how to utilize models for operational seasonal prediction. Table 2 summarizes the relationships for the tropical Pacific region and compares the GCM results to the observations of RH. Most areas compare well with the observations. The largest differences in the Pacific occur in the region of Fiji, as discussed above. Table 2 also shows that in the central Pacific the observed SO-related anomalies are larger than the model anomalies.

In some regions where there are enough observed data to detect signals, the observations do not show strong SO-related anomalies, but the model does. For example, in the GCM, northwestern North America shows drier-than-normal conditions associated with a high index for both halves of the year, and northeastern North America shows wetter-than-normal conditions associated with a high index for the Apr(0)–Sep(0) season.

During Apr(0)–Sep(0), there is a symmetric model relationship in the eastern Mediterranean. A similar relationship was found by Ropelewski and Halpert (1987). However, since that is the dry season for the region, no further analysis was performed. There is a wet season model relationship in the Mediterranean region for high-index periods (Fig. 1) and a weaker opposite relationship in the region associated with a low index (not shown). For these regions in which inconsistencies occur, the GCM is consistently too sensitive to the SST forcing. Further study of the observations is needed to determine whether or not there is any validity to the model signals in these regions. As the GCMs improve, we expect that they may suggest additional areas for further observational and model validation studies.

Another inconsistency is the GCM bias, which is shown by a general tendency for stronger model signals associated with the high index (Fig. 1). Geographical shifts in the model response compared to the observations are also common, such as over the Gulf of Mexico region, in the southwestern Pacific, and over southern India. These types of regional shifts are not surprising, based on numerical weather prediction experience (e.g., Graham et al. 1994; Livezey et al. 1997).

However, the atmospheric GCM SO-related percentiles are generally consistent with the observations. We can expect some SO-related forecast skill from the coupled model over many global regions, provided that the SST is adequately forecast. This study points out the importance of observations to the interpretation of seasonal model forecasts for the identification of biases in precipitation amounts and locations. With the development of satellite-based precipitation observations, such comparisons have become possible (e.g., Arkin and Ardunay 1989). Other potential uses of this study include the identification of data-sparse regions where more observational study is needed; and suggesting where the SO may be a factor for some, but not all, SO episodes.

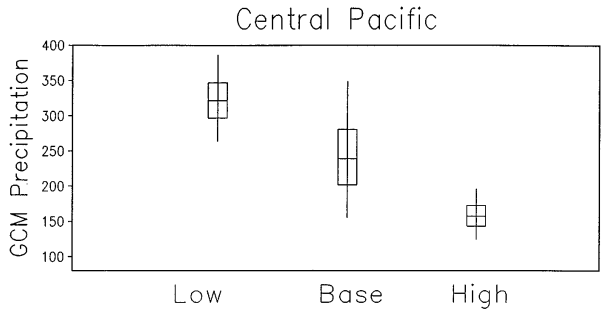

FIG. 7. As in Fig. 4 except for the central Pacific. The averaging season is Mar(0)–Mar(+).

Acknowledgments. We thank M. Masutani for making the model output available; M. Halpert, A. Kumar, and R. Livezey for discussions; and J. Huang for programming help. This work was partially supported by the National Oceanic and Atmospheric Administration Office of Global Program's Pan-American Climate Studies program.

REFERENCES

Arkin, P. A., and P. E. Ardunay, 1989: Estimating climatic-scale precipitation from space: A review. *J. Climate,* **2,** 1229–1238.

Chu, P.-S., 1991: Brazil's climate anomalies and ENSO. *Teleconnections Linking Worldwide Climate Anomalies*, M. Glantz, R. W. Katz, and N. Nicholls, Eds., Cambridge University Press, 43–71.

Graham, N. E., T. P. Barnett, R. Wilde, M. Ponater, and S. Schubert, 1994: On the roles of tropical and midlatitude SSTs in forcing interannual to interdecadal variability in the winter Northern Hemisphere circulation. *J. Climate,* **7,** 1416–1441.

Janowiak, J. E., and P. A. Arkin, 1991: Rainfall variations in the Tropics during 1986–1989, as estimated from observations of cloud-top temperature. *J. Geophys. Res.,* **96** (Suppl.), 3359–3373.

Ji, M., A. Kumar, and A. Leetmaa, 1994: An experimental coupled forecast system at the National Meteorological Center. Some early results. *Tellus,* **46A,** 398–418.

Kiladis, G. N., and H. F. Diaz, 1989: Global climatic anomalies associated with extremes in the Southern Oscillation. *J Climate,* **2,** 1069–1090.

Kumar, A., M. Hoerling, M. Ji, A. Leetmaa, and P. Sardeshmukh, 1996: Assessing a GCM's suitability for making seasonal predictions. *J. Climate,* **9,** 115–129.

Livezey, R. E., M. Masutani, A. Leetmaa, H. Rui, M. Ji, and A. Kumar, 1997: Teleconnective response of the Pacific–North American region atmosphere to large central equatorial Pacific SST anomalies. *J. Climate,* **10**, 1787–1820.

Rasmusson, E. M., and T. H. Carpenter, 1983: The relationship between eastern equatorial Pacific sea surface temperatures and rainfall over India and Sri Lanka. *Mon. Wea. Rev.,* **111,** 517–528.

Reynolds, R. W., and T. M. Smith, 1994: Improved global sea surface temperature analyses using optimum interpolation. *J. Climate,* **7,** 929–948.

Ropelewski, C. F., and M. S. Halpert, 1987: Global and regional scale precipitation patterns associated with the El Niño/Southern Oscillation. *Mon. Wea. Rev.,* **115,** 1606–1626.

——, and ——, 1996: Quantifying Southern Oscillation–precipitation relationships. *J. Climate,* **9,** 1043–1059.

Shukla, J., and D. A. Paolino, 1983: The Southern Oscillation and long range forecasting of the summer monsoon rainfall over India. *Mon. Wea. Rev.,* **111,** 1830–1837.

Smith, T. M., R. W. Reynolds, R. E. Livezey, and D. C. Stokes, 1996: Reconstruction of historical sea surface temperatures using empirical orthogonal functions. *J. Climate,* **9,** 1403–1420.